Climate Dynamics (2022) 59:2871–2886
https://doi.org/10.1007/s00382-022-06250-z

# Quantifying the role of the large-scale circulation on European summer precipitation change

**Hylke de Vries[1] · Geert Lenderink[1] · Karin van der Wiel[1] · Erik van Meijgaard[1]**

Received: 13 September 2021 / Accepted: 8 March 2022 / Published online: 29 March 2022


**Abstract**
Regional climate projections indicate that European summer precipitation may change considerably in the future. Southern Europe can expect substantial drying while Northern Europe could actually become wetter. Model spread and internal variability in these projections are large, however, and unravelling the processes that underlie the changes is essential to get more confidence in these projections. Large-scale circulation change is one of the contributors to model spread. In this paper we quantify the role of future large-scale circulation changes to summer precipitation change, using a 16-member single-model ensemble obtained with the regional climate model RACMO2, forced by the global climate model EC-Earth2.3 and the RCP8.5 emission scenario. Using the method of circulation analogues three contributions to the future precipitation change are distinguished. The first is the precipitation change occurring without circulation change (referred to as the thermodynamic term). This contribution is characterised by a marked drying-to-wetting gradient as one moves north from the Mediterranean. The second contribution measures the effects of changes in the mean circulation. It has a very different spatial pattern and is closely related to the development of a region of high pressure (attaining its maximum west of Ireland) and the associated anti-cyclonic circulation response. For a large area east of Ireland including parts of western Europe, it is the major contributor to the overall drying signal, locally explaining more than 90% of the ensemble-mean change. In regions where the patterns overlap, the signal-to-noise ratio of the total change is either enhanced or reduced depending on their relative signs. Although the second term is expected to be particularly model dependent, the high-pressure region west of Ireland also appears in CMIP5 and CMIP6 ensemble-mean projections. The third contribution records the effects of changes in the circulation variability. This term has the smallest net contribution, but a relatively large uncertainty. The analogues are very good in partitioning the ensemble-mean precipitation change, but describe only up to 40% of the ensemble-spread. This demonstrates that other precipitation-drivers (SST, spring soil moisture etc.) will generally strongly influence trends in single climate realisations. This also re-emphasises the need for large ensembles or using alternative methods like the Pseudo Global Warming approach where signal to noise ratios are higher. Nevertheless, identifying the change mechanisms helps to understand the future uncertainties and differences between models.

**Keywords** Summer precipitation change · Europe · Climate change · Circulation response · Thermodynamic response

## 1 Introduction

The European summer precipitation climate may change considerably in the future following anthropogenic climate change (Meehl et al. 2007; Polade et al. 2014; Coumou et al. 2018). Most of southern Europe can expect significant drying, while northern and higher-altitude regions may respond differently and could even become wetter. Future climate precipitation projections come with large uncertainties because many factors influence precipitation formation (e.g., radiation, soil-moisture, large-scale circulation, relative humidity, vertical stability) and most of them are projected to change (O'Gorman and Schneider 2009; Fowler et al. 2021). This complexity, combined with natural variability—known to be rather large for precipitation—mean that climate model projections can be quite divergent. Bladé et al. (2012) demonstrated that climate models do not necessarily represent the precipitation producing mechanisms correctly, while (van Haren et al. 2012) showed that biases

✉ Hylke de Vries
hylke.de.vries@knmi.nl

[1] Royal Netherlands Meteorological Institute, De Bilt, The Netherlands

in large-scale SST and circulation statistics can explain discrepancies between modelled and observed precipitation (van Ulden and van Oldenborgh 2006). Near land-sea borders the mechanisms may be so sensitive to local conditions that even a high resolution regional climate model (RCM) may have problems resolving them (e.g. Lenderink et al. 2009; Attema and Lenderink 2014).

To understand the pattern of future precipitation change, one clearly needs to unveil the mechanisms in a background dominated by natural variability (Rowell and Jones 2006; Polade et al. 2014; Pfahl et al. 2017; Norris et al. 2019). Literature on the subject is abundant. Generally, two main categories are distinguished, thermodynamic and dynamic mechanisms (e.g. Rowell and Jones 2006; Norris et al. 2019), although exact definitions vary. Examples of the latter are changing stormtracks, the northward expansion of the Hadley cell and pressure adjustments to large-scale sea-surface temperature (SST) gradients. Rowell and Jones (2006) went beyond two categories by distinguishing four drivers/mechanisms: more rapid decline of soil moisture in spring, a larger land-sea contrast in lower tropospheric summer warming leading to air of lower relative humidity when advected over land, other large-scale atmospheric changes (including circulation changes), and finally a positive feedback between soil moisture and rainfall. With dedicated model experiments they find different mechanisms are important in different regions in Europe: thermodynamic processes in the South, while further north dynamic influences also contribute. van Haren et al. (2015) showed that increased horizontal resolution in global climate model (GCM) experiments influences the role of the circulation. More recently Brogli et al. (2019b) found seasonality in the mechanisms, but confirmed the dominant role of thermodynamic changes in Mediterranean summer. In Brogli et al. (2019a) the various driving mechanisms were isolated using a carefully designed set of regional climate model simulations in combination with a so-called Pseudo Global Warming (PGW) approach (Schär et al. 1996). In a PGW experiment one forces a regional climate model with present-day circulation variability at the boundaries, but simultaneously adds a time-constant or seasonally varying delta-change signal obtained from e.g. a climate ensemble such as CMIP6.

The present study revisits the subject of the role of the large-scale circulation on summer future precipitation changes. The standard summer season (June–July–August, JJA) is used. Because of the large natural variability, we use an ensemble of climate model simulations, obtained with EC-Earth GCM (Hazeleger et al. 2012) and dynamically downscaled with RACMO RCM for the RCP8.5 emission scenario (van Meijgaard et al. 2008, 2012).

Our aim is to quantify to what extent changes in the large-scale circulation contribute to the regional precipitation-change pattern over Europe in summer and to the overall uncertainty of this estimate. In most places, but especially in coastal areas and in regions with steep topography, the circulation exerts a large influence on precipitation. Just as a small change in wind direction can turn a dry Alpine valley into a wet one, we expect that subtle changes in the mean and variability of the large-scale circulation will leave a distinct footprint in the precipitation field. Using a large ensemble is essential to examine the changes quantitatively in their competition against natural variability (Deser et al. 2020; Lehner et al. 2020; Wood et al. 2021). Saffioti et al. (2017) demonstrated (albeit for the winter) that accounting for circulation variability may dramatically improve consistency of modelled precipitation trends. This was reaffirmed by Fereday et al. (2018) who found that the uncertainty in the future circulation change is a major contributor to the total uncertainty. Thereby our subject is intricately linked to the subject of dynamical adjustment, in which machine-learning techniques like (regularised) ridge regression have recently shown to be highly promising (Sippel et al. 2019).

In this study circulation-induced effects are identified using a method based on circulation analogues. These are defined as (atmospheric) states that are similar to another state given some similarity metric (Yiou 2014; Clemins et al. 2019). The large-scale (i.e. GCM-based) mean sea level pressure field (MSLP) is used, which is a subjective, but widely used choice (e.g. van Haren et al. 2015). By modifying the analogue technique we are able to discriminate between circulation effects predominantly associated with a change of the mean, and those finding their origin in altered variability (Van der Wiel and Bintanja 2021).

The outline of the paper is as follows. Sections 2 and 3 introduce data and methodology. Main results are discussed in Sect. 4. In section 5 we briefly explore alternative methods. Section 6 connects the framework to PGW experiments. Conclusions and final remarks are presented in Sect. 7. A number of additional figures is included in the supplementary material.

## 2 Data

The main data source in this study is the 16 member GCM/RCM (EC-Earth2.3/RACMO2) initial condition ensemble (Hazeleger et al. 2012; van Meijgaard et al. 2008, 2012; Aalbers et al. 2018). This ensemble comprises 16 simulations (period 1850–2100 for the GCM (atmospheric spectral truncation at T159, corresponding to ~125 km resolution), dynamically downscaled with RACMO2 RCM (0.11 degree resolution, around ~12 km) over western central Europe for the period 1950–2100) and forced for the period after 2005 by the RCP8.5 emission scenario (Meinshausen et al. 2011). Main variables discussed are summer (JJA) daily precipitation and mean sea level pressure (MSLP), but incidentally we will refer

to other climate variables. Model precipitation is briefly compared to the gridded E-OBS v23.1e precipitation data (Cornes et al. 2018). We study the differences between a present-day period (C, 1991–2020, the most recent 30-year period) and a future period (F, 2071–2100). To make the results more easily comparable to studies that use a different reference period, the future changes are scaled by the ensemble-mean increase of the GCM global temperature (3.1 K). For precipitation change we mostly show the relative change per degree global warming (units: %/K).

The geographical area for the analogues is 30 W–40 E and 40–70 N. This region was chosen because Western Europe is our primary area of interest. Shifting the domain five degrees south and shrinking it in the east–west direction by ten degrees did not have major impact our main results. Two further preprocessing steps are performed prior to computing the analogues. First MSLP (always taken from the GCM) is regridded bilinearly to a 2.5 × 2.5 degree regular latitude × longitude grid. Secondly the analogues are computed using anomaly fields, obtained by subtracting a monthly-mean seasonal cycle of the control period. The MSLP field is not detrended since our aim is to diagnose circulation changes from the MSLP trend. Other climate variables are shown on native grid and do not require any preprocessing. Only when RCM and GCM are compared quantitatively, the final GCM result is interpolated to the RCM grid using conservative remapping.

## 3 Circulation-analogue framework

In this section we derive the general circulation-analogue framework that is used to quantify the impact of atmospheric circulation changes on climate variables like precipitation and temperature.

### 3.1 Three-component decomposition

The average state of a climate variable $X$ (such as precipitation) in the control and future climate are denoted by $C$ and $F$ respectively. In this study, the future change $\Delta X = F - C$, is decomposed as

$$\Delta X = \Delta X_{TD} + \Delta X_{CM} + \Delta X_{CV} + \delta \quad (1)$$

Each term in Eq. (1) and subsequent equations implicitly carries a label indicating the ensemble member. The first term on the right-hand-side of Eq. (1) records changes occurring in absence of circulation change, and is referred to as the *thermodynamic* (TD) term (e.g. Pfahl et al. 2017; Lenderink et al. 2019). The second and third term measure contributions from changes in the large-scale mean circulation (CM) and its variability (CV) respectively. The $\delta$-term collects a remaining part left unexplained by the analogues. It is a variability-producing term related to precipitation drivers different from large-scale circulation, as well as to errors made by the analogues (more details below). Unlike e.g. Brogli et al. (2019a) we do not distinguish sub-classes in the thermodynamic term.

### 3.2 Definition of the analogues

A circulation analogue is defined as a reconstruction of the MSLP time-series of a given period of a given member of the ensemble. The MSLP field connects to the large-scale circulation via the geostrophic wind relation (Holton 1979). The analogue is found by minimising for each day the Euclidean distance of the MSLP anomaly difference field with all other days from all ensemble members within the same season (JJA). Using days outside the season was found to systematically bias the response (especially in the Mediterranean region because of the asymmetry in the seasonal cycle). Other fields (in our case precipitation) are taken from this reconstruction.

If the analogue is created for the same period as the original, we use the term *equal-period analogue* (EPA) and notation $C^e$ for the present-day and $F^e$ for the future. For the EPA of member-$j$ all members except member-$j$ are used. Similarly, $F^a$ is defined as the future average state (of $X$) after matching the circulation statistics of the future state to those of the present-day simulation. Now all members can be used. Likewise $C^a$ is the present-day average state of $X$ in response to future-day circulations. $F^a$ and $C^a$ will be referred to as the "type-a" forward and backward analogues respectively. The 'backward' analogue is needed because, as will be explained below, using forward analogues only will bias our results.

Using these "type-a" analogues one can separate the thermodynamic component from the circulation-change components (derivation in Sect. 3.4). To subdivide the circulation-change components these type-a analogues have to be augmented with a second set. In this second "type-b" set (denoted by $F^b$ and $C^b$) the (ensemble) mean circulation change is added to the circulation patterns from the present-day prior to matching these to the future patterns. The type-b analogues thereby contain *both* the thermodynamic (TD) and the mean circulation-change (CM), but *not* the possible change of the circulation variability (CV). In this way, $F^b$ for example has future thermodynamics and future mean circulation, but present-day circulation variability.

### 3.3 Properties of the analogues

By construction the analogue MSLP resembles the direct model output MSLP as closely as possible. However, the matching is not perfect. Errors are partly random mismatches that average out, but there is also a systematic component that may impact the target field (in our case precipitation). For example, the matching algorithm has a tendency to

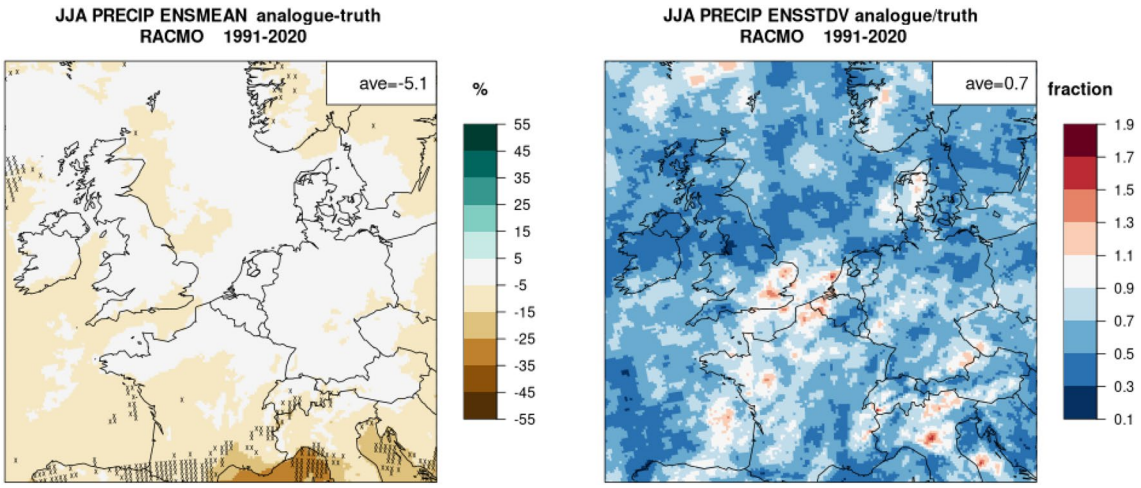


**Fig. 1** (left) Dry bias of the EPA in RACMO, computed as $\langle C^e - C\rangle / \langle C\rangle$ (crossed where outside the 95% ensemble spread). (right) Ratio of ensemble standard deviations $sd(C^e)/sd(C)$

'zoom in' on the Atlantic where MSLP variability is largest. The relative error between analogue and model MSLP is small in this region (Supplemental Fig. S1), but increases further south and towards the edges of the domain. In addition, when searching for an analogue of an MSLP field that contains (multiple) small-scale weather features, the algorithm may favour a field with fewer large-scale and thereby smoother structures over one with multiple smaller-scale, but slightly displaced structures (double-penalty problem). As a result the daily MSLP variability of the analogues is reduced (top-right panel in Fig. S1).

We have experimented with improving the quality of the analogues in two ways. First we reduced the domain over which the MSLP analogues are obtained. This locally improves their quality. Another option is to downweight regions where MSLP variability is large by using MSLP/sd (MSLP) for the analogue construction. This also improves the analogues, but it has as a disadvantage that spatial correlations are reduced, which obscures the subsequent interpretation. In the end we decided to stay with the simplest approach (i.e., use one single large analogue-domain and no prior standardization) but provide information on the implication of the method's limitations for the associated precipitation field. Two of these are discussed now.

*Dry bias* We define $\varepsilon^e_C$ ($\varepsilon^e_F$) as the difference between the control (future) EPA and the direct model output

$$\varepsilon^e_C = C^e - C, \quad \varepsilon^e_F = F^e - F. \tag{2}$$

Below, we use $\langle\cdot\rangle$ notation to indicate that an ensemble average has been taken. The ensemble-mean deviations $\langle\varepsilon^e_C\rangle$ and $\langle\varepsilon^e_F\rangle$ are referred to as the *bias* of the control and future EPA. They measure the bias inherent to the method of analogue selection. Especially in the Mediterranean a considerable fraction of the precipitation is formed as a result of smaller-scale circulation features and processes not seen by the analogue machinery. A consequence of the double penalty is that the control EPA has a dry bias (Fig. 1, left panel; see Fig. S2 for EC-Earth). The future EPA has a similar bias (not shown).

*Ensemble spread and "regression to the mean"* The ensemble spread in the analogue precipitation differs from the direct model output (Fig. 1, right panel), with a 30% reduction on average. At least two reasons can be given for this reduction. First, circulation variability is not the only source of precipitation variability. Other drivers (SST, spring soil-moisture preconditioning, changes in relative humidity etc) may also be important, especially at lower latitudes and over the Mediterranean where circulation variability is smaller than over the Atlantic. In the reconstruction, analogue states are sampled from the *entire* ensemble. Therefore the analogues will 'regress towards the mean' for these other drivers, which tends to reduce the ensemble spread. Incidentally this 'regression to the mean' effect is also the reason why for an individual ensemble member $[C^e]_i$ as defined above will generally be quite different from $[C]_i$, regardless of the presence of an overall bias. Another reason for the reduction in the ensemble spread is the dry bias itself. If it systematically rains too little in the analogues, this is likely to impact the precipitation variability.

### 3.4 Contributions

The components of the right-hand-side of Eq. (1) take the form of particular sums and differences of the various types

**Table 1** Contribution to the precipitation of the various types of fields used in this study

| Component | Notation | Contribution | | |
|---|---|---|---|---|
| | | $X_{TD}$ | $X_{CM}$ | $X_{CV}$ |
| Direct model output | $C, F$ | $C_i, F_i$ | $C_i, F_i$ | $C_i, F_i$ |
| EPA (equal-period) | $C^e, F^e$ | $\tilde{C}, \tilde{F}$ | $C_i, F_i$ | $C_i, F_i$ |
| Type-a analogue | $C^a, F^a$ | $\tilde{C}, \tilde{F}$ | $F_i, C_i$ | $F_i, C_i$ |
| Type-b analogue | $C^b, F^b$ | $\tilde{C}, \tilde{F}$ | $C_i, F_i$ | $F_i, C_i$ |

The left column indicates the component. The other columns indicate the contribution from each term, where a ~ above a term indicates it is "regressed to the mean" and a subscript $i$ indicates "similar to an ensemble member"

of analogues and direct model output. A heuristic derivation is now given.

*Thermodynamic contribution* Because $F^a$ is the future analogue under control (C) circulation conditions, $F^a - C$ seems a good candidate to describe the future precipitation change in absence of circulation change, i.e., what we refer to as the TD-term. However, by writing $(F^a - C)$ as $(F^a - C^e) + (C^e - C)$ one can see immediately that only $(F^a - C^e)$ is a future-change term. The contribution $(C^e - C)$, equal to $\varepsilon_C^e$ following Eq. (2) (with ensemble average equal to the bias) is related to the variability of precipitation drivers other than the large-scale circulation. We exclude this term from the TD-term. If $(F^a - C^e)$ is a suitable 'forward' estimate of the thermodynamic contribution, it is easy to show that $(F^e - C^a)$ is an equally suitable 'backward' estimate. We write

$$\Delta X_{TD}^{fw} = (F^a - C^e), \quad \text{(forward-only)} \tag{3a}$$

$$\Delta X_{TD}^{bw} = (F^e - C^a). \quad \text{(backward-only)} \tag{3b}$$

For a given ensemble member the forward and backward terms are not identical—they are, for example, based on different circulation climates. Because there is no preference for Eq. (3a-b) we take the average to define the TD-component. Note that the sum of the two"left-over"variability-producing terms, $(F - F^e) - (C - C^e)$ does classify as a proper future-change term that is almost independent of circulation change. It could therefore be grouped under the "thermodynamic"(i.e. non-circulation related) response terms. As we will see in the following sections, it has only a small net contribution, but is a major factor in increasing uncertainty in the future change.

*Circulation contributions* A similar reasoning can be used to 'derive' the circulation components, keeping in mind to only use analogue pairs as differences. Table 1 may be used to find suitable combinations. It summarises the specific contributions of each analogue type. In this way we obtain $(F^b - F^a)$ and $(C^a - C^b)$ for respectively forward and backward estimates of $\Delta X_{CM}$, and $(F^e - F^b)$ and $(C^b - C^e)$ for $\Delta X_{CV}$.

*Final equations* After averaging the forward and backward estimators of the various terms we arrive at

$$\Delta X_{TD} = \left[(F^a - C^e) + (F^e - C^a)\right]/2, \tag{4a}$$

$$\Delta X_{CM} = \left[\left(F^b - F^a\right) + \left(C^a - C^b\right)\right]/2, \tag{4b}$$

$$\Delta X_{CV} = \left[\left(F^e - F^b\right) + \left(C^b - C^e\right)\right]/2. \tag{4c}$$

Combining Eqs. (1) and (4) gives

$$\delta = (F - F^e) - (C - C^e) \tag{5}$$

which is of course nothing but the sum of the two "left-over" variability-producing terms, that were related to processes that can not be distinguished using analogues, and therefore had been excluded on purpose. The $\delta$-term is an important source of variability in the precipitation trend, associated with the natural variability of all precipitation drivers other than the large-scale circulation.

The systematic bias is still included in Eq. (4). Fortunately the analogues appear only in the form of differences, making them less sensitive to the bias itself. Still one may consider applying a form of bias adjustment. In the appendix we derive a set of bias-adjusted Eqs. (8–9). These will be the equations on which the main results are based. Finally, note that the decomposition can be understood easily by writing $(F - C) = (F^a - C^e) + (F^b - F^a) + (F^e - F^b) + [(F - F^e) + (C^e - C)]$ (forward-only), and likewise $(F - C) = (F^e - C^a) + (C^a - C^b) + (C^b - C^e) + [(F - F^e) + (C^e - C)]$ (backward-only). The decomposition is a physically motivated way of linearly adding and subtracting terms.

## 4 Results

This section discusses the main results. We first describe the present-day climatology in the RCM (RACMO) and GCM (EC-Earth). This is followed by an analysis of the future changes and the three-component decomposition.

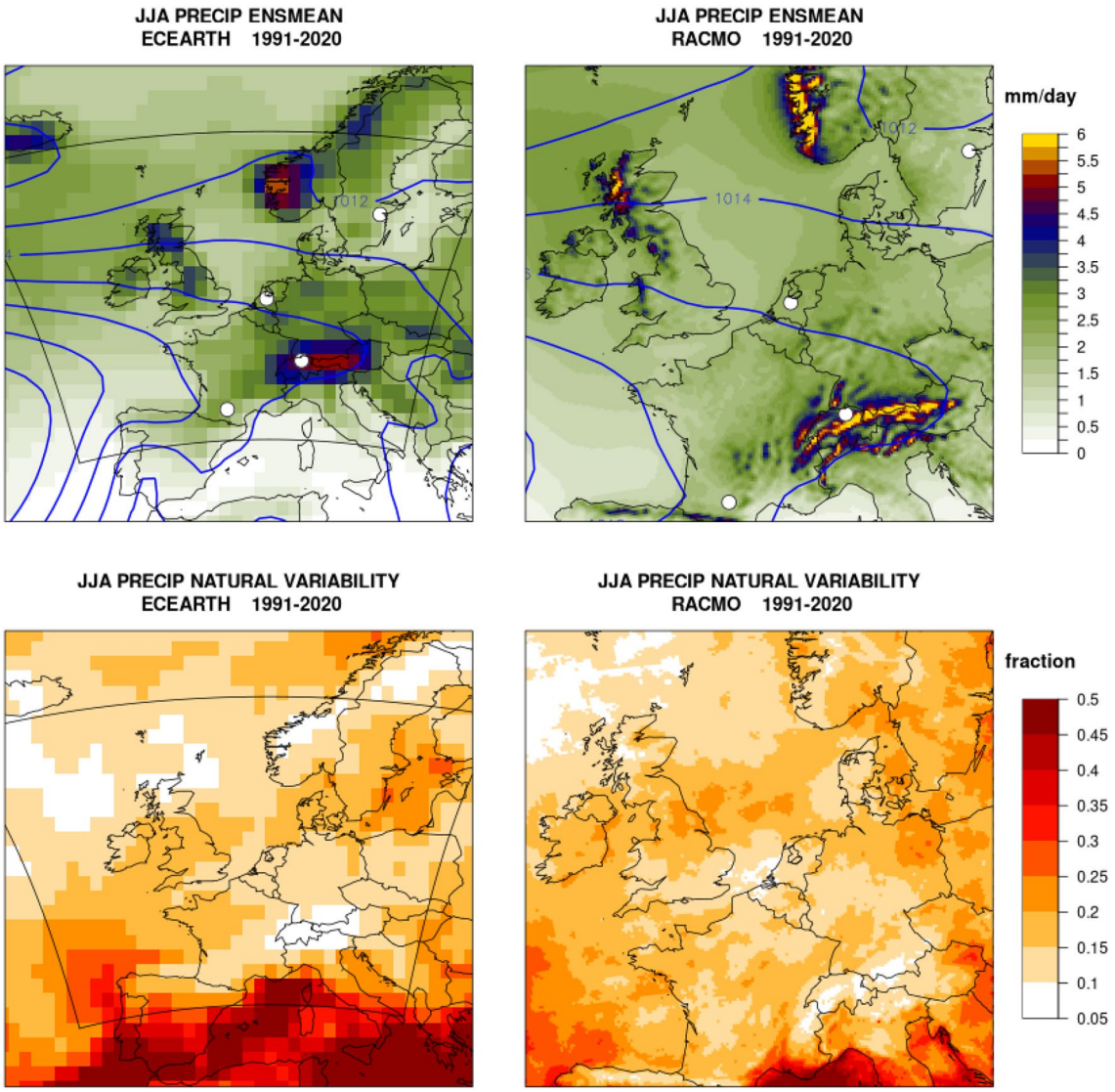


**Fig. 2** (top row) Mean summer precipitation [mm/day] in present-day climate; (bottom row) amplitude of natural variability (3.28 times ensemble standard deviation divided by ensemble mean) for GCM (left) and RCM (right). Contours indicate the MSLP (every 2 hPa). The thin line marks the inner domain of the RCM. Dots show locations discussed in Sect. 4.5

## 4.1 Present-day climate

Figure 2 shows the summer precipitation climate for the present-day period for both GCM and RCM. High-altitude regions stand out and are much wetter than regions at lower elevation. The Mediterranean area is particularly dry (and warm). Figure S7 shows the EC-Earth climatology of a few other relevant parameters. Around the Mediterranean the soils in EC-Earth are quite dry, as a result of which JJA evaporation rates are generally lower than further north, despite the little cloud cover and abundant sunshine. GCM and RCM precipitation patterns are structurally similar, with the latter providing more detail. The RCM is wetter over western land-sea borders and over steep topography (e.g. Chen and Knutson 2008). Also over the North Sea there is more precipitation in the RCM, whereas land regions are generally drier (see also top-left panel in Fig. S6). Compared to E-OBS gridded observations EC-Earth is too wet over most of the land area; in RACMO mostly the mountainous regions are too wet (Fig. S3). Note, however, that E-OBS may be systematically too dry over mountainous regions (Vautard et al. 2021).

The bottom panels in Fig. 2 show the natural variability within the ensemble at the 30-year time scale (It is measured as 3.28 times the ensemble standard deviation divided by the ensemble mean. This corresponds to the approximate 95% range if the distribution of the 30-year means is Gaussian). Even on this long time scale the amplitude of

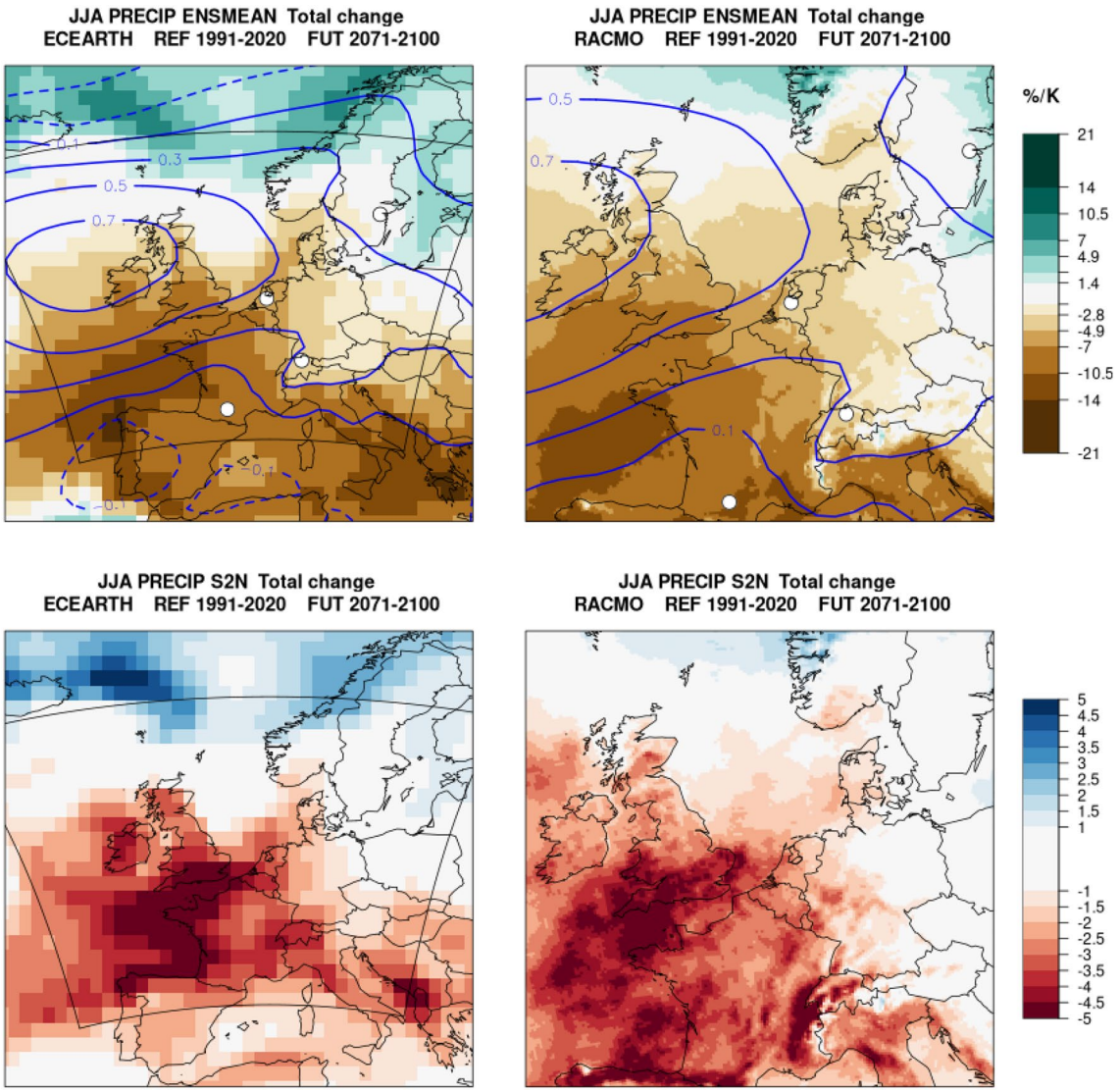


**Fig. 3** (top row) Total fractional change of summer precipitation per degree global warming [%/K]; (bottom row) Signal-to-noise (the change of mean divided by ensemble standard deviation) for GCM (left) and RCM (right). Contours show MSLP trend per degree global warming (interval 0.2 hPa/K)

the natural variability is substantial (10–20% of the ensemble-mean in most regions). The Mediterranean stands apart. Owing in part to the very small mean values found in the region, it displays a much larger natural variability, locally exceeding 50%. Ensemble spread in GCM and RCM are comparable, with the latter being more patchy.

## 4.2 Total future change

Future changes of summer precipitation and MSLP are shown in Fig. 3. Results are scaled by the mean increase in global temperature of 3.1 K. Most eye-catching is the north-south gradient in the pattern. In the North (and at higher elevations) modest precipitation increases are found, especially in the GCM (left panel). Towards lower latitudes the sign changes, and substantial drying of locally more than 15% per degree global warming is found, coinciding with enhanced warming (see Fig. S4 for the warming signal in RACMO), reductions in relative humidity and cloudcover and increases in shortwave radiation (see Fig. S8 for changes in the fields in EC-Earth). The GCM and RCM patterns are rather similar (van Haren et al. 2015). The RCM is slightly wetter than the GCM over the North Sea in the current climate (Fig. 2) and also shows a stronger decrease in this region (For completeness Fig. S6 quantifies these differences, but given their small amplitude we do not attempt to interpret them).

The MSLP change (contours) shows a large-scale pressure increase, that attains its maximum west of Ireland. Its

effect on precipitation is to modify the general north-south wet-dry pattern substantially (discussed in the next section). The origin of the MSLP pattern is thought to be related to the response of the North Atlantic to climate change (Haarsma et al. 2015). In EC-Earth (and in many other GCMs), the temperature of the North Atlantic increases less rapidly than the global mean. This has been shown to be related to a slowdown of the Atlantic Meridional Overturning Circulation (AMOC) (Haarsma et al. 2015). Associated with the lagged warming of the North Atlantic (Fig. S4), a high-pressure region gradually is formed east of the 'warming hole'. For EC-Earth it reaches a maximum west of Ireland. Compared to the typical amplitude of a daily weather pattern, its amplitude is rather modest (less than one hPa per degree global warming), but its impact on precipitation is felt nevertheless in a large region to the east. Maximum decreases are found in a broad region off the coast of France, Spain and Portugal, as well as in the south of Italy. The RCM replicates this signal quite well. Finally, in the GCM this region displays signs of the formation of a so-called "heat low" (Haarsma et al. 2009), related to the strong heating of the area.

The signal-to-noise ratio (S2N, determined here as the ensemble mean change divided by the ensemble standard deviation) is shown in the bottom panels of Fig. 3. White masking is used for regions where the absolute value of S2N is smaller than unity[1] and blue/red colors are used to indicate a robust wetting/drying signal. Not to a complete surprise, the south-west part of the domain displays the highest S2N values. Further to the east and especially to the north the S2N reduces. The S2N of the RCM is in most places somewhat smaller than that of the GCM, and also more patchy. Notable exceptions are mountain regions where the RCM displays a very high S2N. For a broad region in western and central Europe S2N is not very high. Note that in this study we consider future differences obtained for the rather strong RCP8.5 emission scenario and for two periods that are far apart in time. For the lower RCP4.5 scenario or for time periods that are closer together, the S2N will be reduced.

### 4.3 Future change from analogues

In Sect. 3.3 it was shown that the present-day EPA has a dry bias (Fig. 1). The future EPA has a similar bias (not shown). Figure 4 shows that despite these biases the analogues capture the ensemble-mean future precipitation change quite well in most of the area (The GCM result is in the top-right panel of Fig. S2). The smallness of $\delta$ has two implications. Firstly the results of the final decomposition Eqs. (4–5) to be discussed next will not be influenced strongly by the bias-adjustment (in fact only the TD-component is affected by the bias adjustment discussed in Eq. (8)). Secondly, processes unresolved by the analogues mostly average out in the ensemble mean. As before, the largest errors are found in the Mediterranean and off the coast of Portugal, where the analogues underestimate the drying.

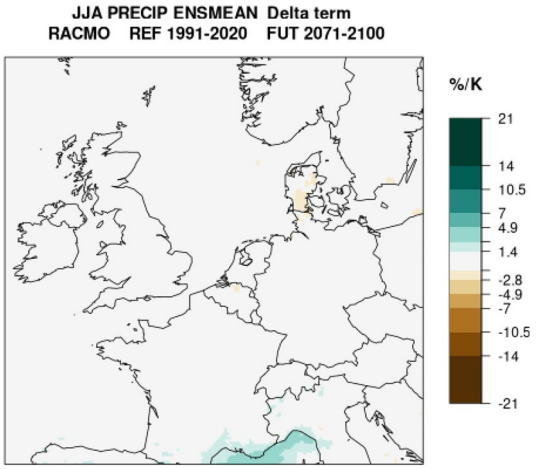


**Fig. 4** Ensemble-mean difference between EPA-based change and full change $(F^e - C^e) - (F - C) \equiv -\delta$ for RACMO RCM

### 4.4 Thermodynamic- and circulation-contributions

Using the method of circulation analogues, as explained in Sect. 3, one can separate the total precipitation change pattern into contributions from circulation-change and thermodynamics. The circulation is further decomposed into a term related to the mean-circulation change and one that may pick up signals from changes in weather-pattern variability, altered persistence of weather patterns etc.

The panels in Fig. 5 show this decomposition for the RCM (The GCM results are in Fig. S5). The thermodynamic and mean-circulation patterns are rather different, confirming that the partitioning approach has actually worked. Partitioning schemes in which one isolates contributions by adding and subtracting terms, like Eq. (1), may introduce artificially compensating contributions in the different terms. This seems not a major issue here. The GCM results are quite similar and thereby serve as a coarse-grained validation.

The thermodynamic pattern is more zonally oriented than the total change pattern (Fig. 3), with robust drying in the south, and a gradual change towards wetting further north. In a broad latitudinal band the thermodynamic contribution is almost zero. The thermodynamic term in the south is also

[1] For simplicity we use unit S2N. It can be shown that the less strict requirement of $|S2N| \geq 0.55$ corresponds to a rejection of the null hypothesis of zero change at 95% confidence (see Sect. 2.4 of Aalbers et al. 2018).

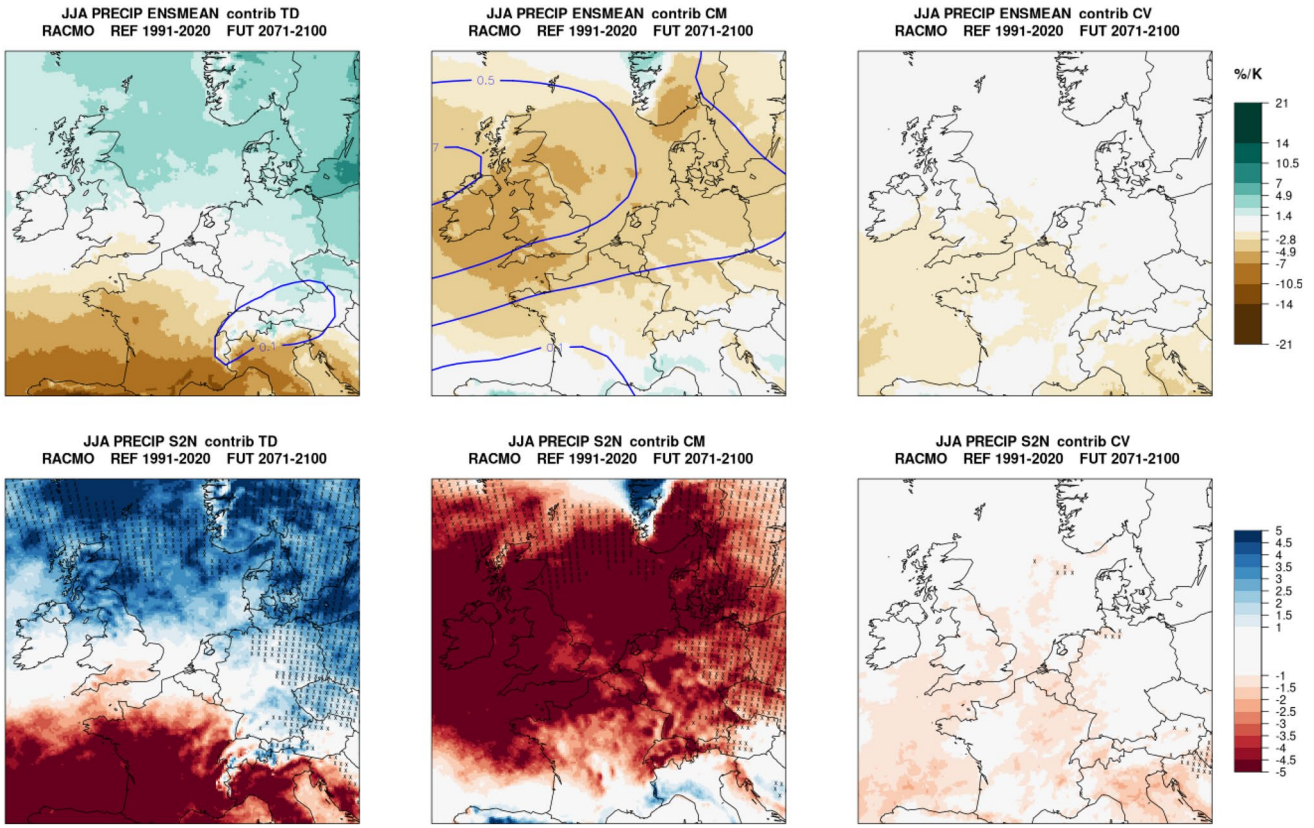


**Fig. 5** Contributions to RCM summer precipitation change per degree global warming (top) and their signal-to-noise ratios (bottom). Contours show change of MSLP in hPa per degree global warming. Crosses indicate the region where the absolute value of S2N of the total change is smaller than one while that of the component exceeds unity. The stippling density has been reduced for clarity

the most prominent cause of the reduction in soil-moisture, cloud cover and relative humidity as well as the increase in short-wave radiation (not shown).

The pattern associated with mean-circulation change (top middle panel) exhibits a drying pattern in the area centered and east of the region where the pressure increase is strongest. In other variables there are associated reductions in cloud cover and relative humidity and a small additional increase in temperature and short-wave radiation (not shown). For a broad zonal band from Ireland towards the Netherlands and Germany, almost the entire drying signal seen in the model is explained from just the change of mean circulation. The mean circulation-change induced drying extends well into Scandinavia and competes in that region with the wetting coming from the thermodynamic component. In the GCM (Fig. S5) the mean circulation component produces small increases towards Spain and the Mediterranean, but this contribution is overwhelmed by the (thermodynamic) drying.

Separating the circulation terms into mean and variance contributions (middle and right panel), shows a complete dominance by the former, at least over land. Off the coast of France a small drying contribution is found from the circulation variability term. In the GCM (Fig. S5) this region extends further south along the coast of Portugal. The daily standard deviation of MSLP also displays a marked reduction in this region (bottom-right panel Fig. S8) suggesting that it could possibly be related to changes in the summer stormtrack. In general there is no signal that altered circulation variability, persistence or other more subtle circulation effects strongly impact the mean precipitation change in summer over land areas in central and western Europe. The most important changes come from the thermodynamic and the mean-circulation contribution.

Most of the difference between the RCM and GCM change patterns are attributed to the thermodynamic term (Fig. S6 bottom row). Only over Scandinavia the contribution from the mean circulation attains a characteristic signal with increases at the upwind side of the mountain range, and stronger drying at the lee side.

Finally, note that the MSLP change associated with the thermodynamic component is not entirely zero even though by construction the MSLP fields have been matched between control and future period by the method. It picks up the localised "heat-low" response over Spain and the

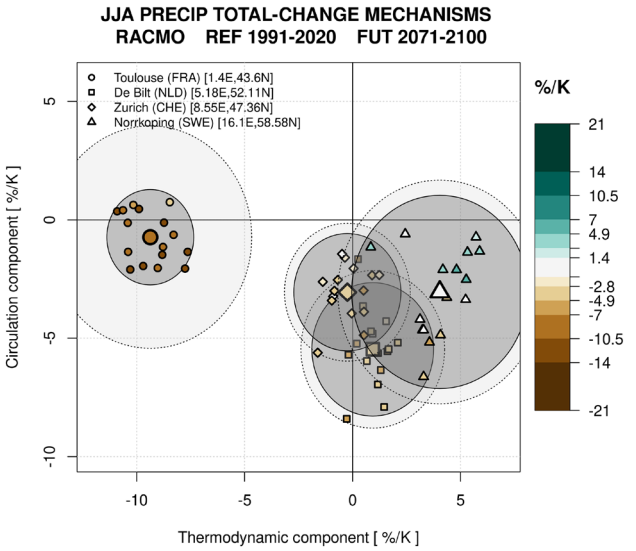


**Fig. 6** Total change of summer precipitation in the RCM for selected locations as a function of the thermodynamic (x-axis) and total circulation (y-axis) contributions. Ensemble-mean/member values are indicated by big/small symbols and color indicates the total change. Dark-grey circles are centered at the ensemble means and have a radius equal to the approximate 95% ensemble spread (computed as $1.64\sigma$ of the analogue contribution). The radius of the light-grey circles denotes the 95% range of the $\delta$-term

Mediterranean and a weak pressure increase over the Alps (Fig. S5). However, its amplitude and spatial scale are much smaller than that seen in the mean circulation change term. Apparently, the pattern is small enough to escape the scrutiny of the analogue finding algorithm. Over the Mediterranean this may be connected to the increase of MSLP-variability (bottom-right panel Fig. S8).

S2N of the thermodynamic and circulation contributions are shown in the bottom panels of Fig. 5. For the TD-term and the CM-term S2N is rather high. Stippling is used to indicate regions where the absolute value of S2N in the total precipitation change is smaller than unity despite the displayed component exhibiting a S2N larger than one. At these locations terms are opposing each other, leading to a smaller total signal and increases in uncertainty.

Both the amplitude and S2N of the CV-term are small. One could consider ignoring this term altogether. It does however have considerable ensemble spread (not shown). In fact, of the two circulation-change terms, it has the largest ensemble spread. The mean-circulation contribution associated with the gradual build up of high pressure is a robust feature of the future ensemble. In contrast, the ensemble members display a much wider range of possibilities regarding circulation-variability changes (with a much smaller ensemble-mean contribution).

### 4.5 Application to specific locations

In this section we have a more detailed look at four locations where the decomposition produces meaningful differences: Toulouse (France), De Bilt (Netherlands), Zürich (Switserland) and Norrköping (Sweden). They can be located via the dots in Fig. 3. Figure 6 shows a scatterplot of the ensemble member contributions to the total precipitation change (color) in terms of their thermodynamic and total circulation contribution (x and y-axis respectively). Dark grey ellipses indicate the approximate 95% ensemble spread of the sum of the analogue-components. The wide, light-grey circles give same range of the $\delta$-term. The ensemble spread in $\delta$ exceeds that of the analogues for all four locations (compare relative radii of the light/dark circles). Therefore, although the large-scale circulation analogues can be used to explain and decompose the ensemble-mean signal, using them to explain the ensemble spread is less successful. Generally we find that only up to 40% of the ensemble spread of the total precipitation change can be explained via variability in the large-scale circulation.

We now discuss some further details. For the southernmost location (Toulouse) the absolute changes are the largest (strong drying) and dominated by the thermodynamic contribution. The circulation contribution has an ensemble average near zero but there is considerable spread between members. A relatively large part of the ensemble-spread in the circulation contribution derives from the CV-term (not shown). Moving north and east, De Bilt and Zürich have a thermodynamic component near zero combined with a negative circulation contribution. For the northernmost of the four locations (Norrköping) the thermodynamic contribution is positive, but the circulation term negative. The opposing signs make the area around Norrköping a region where the net total change is small, but the uncertainty relatively large.

## 5 Alternative methods: using monthly data or Empirical Orthogonal Functions (EOFs)

In the previous sections we have used a circulation-analogue approach based on daily data. The search for the best daily analogues and especially the matching to target response fields, becomes computationally demanding if the ensemble size increases. Therefore we examined whether the main results can also be obtained using monthly data.

When the analogue-computation and partitioning was repeated using monthly-mean data instead of daily data, results very similar to Fig. 5 were obtained, with one exception, the CV-term became even smaller and is essentially included in the CM-term. Therefore, it is likely that much of the CV-term is related to the net effect of changes in

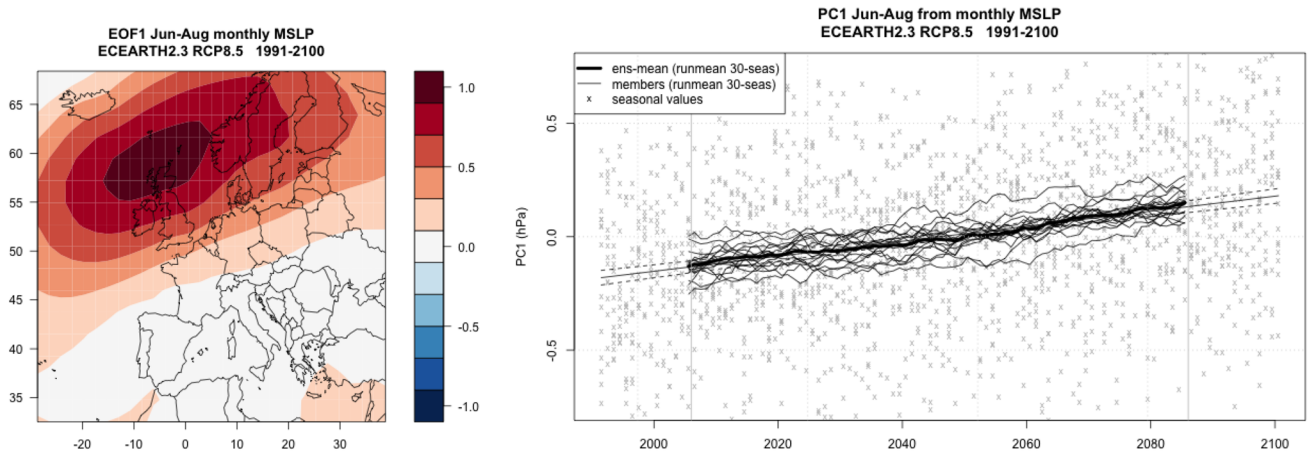


**Fig. 7** (left) Pattern of the first MSLP EOF of JJA (explained variance ~ 33%) and (right) the associated principal component time-series of each member (dots show individual seasons, lines show 30-season running averages) and the ensemble mean (thick line). The linear trend derived from the seasonal averages is also indicated (95% confidence interval dashed). The vertical lines denote the central years of the control and future period

short-term circulation variability (e.g. weather pattern persistence) that can not be 'seen' when using monthly data. However, the basic separation between circulation versus non-circulation terms is diagnosed correctly. Because monthly data is much faster to process this opens the possibility to apply the analogue-machinery easily to other large single-model ensembles or to multi-model intercomparison projects such as CMIP6.

To further examine the robustness of our results, we also tested a completely different method based on Empirical Orthogonal Function (EOF) decomposition. Saffioti et al. (2017) applied a very similar method to the winter season. First we obtained the 10 leading EOFs of monthly JJA MSLP using all ensemble members of EC-Earth, the entire period between 1991 and 2100 and the same domain that was used for the analogues. These 10 EOFs together explain ~95% of the total variance. Figure 7 shows the first EOF-pattern (left) and the associated principal component (PC) time series (right). Although it is primarily a mode of variability, its structure is not unlike that of the total MSLP change field (cf., the contours in Fig. 3). The positive trend in the amplitude (right panel) shows that the pattern strengthens over time, although there is substantial circulation variability (small crosses show seasonal values) even at climatological time scales (thin lines). Similar figures are obtained for the other 9 EOFs (not shown) and together they describe the MSLP trend pattern. The monthly RCM precipitation field is then regressed on to the PC times series (using multiple linear regression and all 10 EOFs). This produces a set of regression maps. Using these regression maps and the PC time series, it is then straightforward to obtain the total circulation-change contribution to the precipitation in the control and future period. Similarly, the CM-term contribution is obtained by using a 30-year running-mean PC time series. Finally the CV-term was defined as the difference between the total circulation contribution and the CM-term. The results are very similar to those obtained using using analogues (see supplemental Fig. S9) and thereby confirm the robustness of the results. Similar to the analogues derived from monthly data, the monthly-based EOF-method does not pick up the small signal of the CV-term.

## 6 Connection to Pseudo-Global-Warming (PGW) experiments

The current framework can be connected to PGW experiments. In such experiments one forces a regional climate model with present-day circulation variability at the boundaries, but simultaneously adds a delta-change signal (e.g, higher temperatures, modified vertical stability etc) (Schär et al. 1996). The difference between a PGW-member and its original contains a combination of the "thermodynamic" change and "mean-circulation" changes. By construction, they do not contain modified large-scale circulation variability. In what way do these simulations differ from the results obtained here? The first important thing to notice is that even though we add a delta-change field, each "futurized" PGW-member will still be in approximately the same state of natural variability as its original. By this we mean that if the original member had anomalously high SST (in the current climate), this would still be the case in the PGW future-analogue etc. The future analogues in this manuscript are different in this respect, as for all precipitation drivers other than circulation they are "regressed to the mean".

In the terminology of the present paper, the state of natural variability of all precipitation drivers except circulation generates a precipitation anomaly (in the current climate) in ensemble member-i equal to $[C - C^e]_i$ (Remember that $[C^e]_i$ is the EPA with present-day circulation statistics as member-i, but all other precipitation drivers "regressed to the mean"). If we now assume that to first order this precipitation anomaly is not changed, the "futurized" PGW-member-i will produce $[F_{PGW}]_i \sim [F^b]_i + [C - C^e]_i - (\langle \varepsilon_F^b \rangle - \langle \varepsilon_C^e \rangle)$, where the last term comes from the bias-adjustment and $[F^b]_i$ is the precipitation corresponding to current-climate circulation variability of member-i but "regressed to the mean" future thermodynamics and mean-circulation (see Table 1). This gives a future change $\Delta X_{PGW}^{fw} \sim F_{PGW} - C = (F^b - C^e) - (\langle \varepsilon_F^b \rangle - \langle \varepsilon_C^e \rangle)$. If a 'reversed-PGW' ensemble is also available, a similar backward expression can be derived. By averaging forward and backward expressions we anticipate that the future change in a PGW experiment will be approximately

$$\Delta X_{PGW} \sim \left[\left(F^b - C^e\right) + \left(F^e - C^b\right)\right]/2 - \left(\hat{\delta}^e + \hat{\delta}^b\right)/2 \quad (6)$$

with $\hat{\delta}^e = \langle \varepsilon_F^e - \varepsilon_C^e \rangle$ and a similar definition for $\hat{\delta}^b$. The final result Eq. (6) is identical to the sum of Eqs. (8a–8b) (or the sum of Eqs. (4a–4b) upon bias adjustment). Because of the absence of the variability producing terms $\delta$ and $\Delta X_{CV}$ the ensemble spread in a PGW ensemble will be much smaller. This is the principal advantage of using PGW. From the analysis shown here we conclude that the error made in such PGW-experiments (i.e. by neglecting the CV-term) for summer precipitation is relatively small.

## 7 Conclusion and discussion

In this paper we have attempted to quantify the large-scale circulation contribution to future precipitation change over Europe in summer. Using a dynamic analogue approach we decomposed the total change signal into a thermodynamic and two circulation contributions, one relating to changes of the mean circulation and one to other circulation changes (such as changes in the circulation variability). The analogue technique was applied to the 16 member EC-Earth/RACMO ensemble. The decomposition, while not perfect, resulted in robust change patterns. Application to GCM and RCM did produce very similar results with the latter producing detail at finer scales. We summarise our main findings.

- Thermodynamic changes (TD-term) and the change of the mean circulation (CM-term), as diagnosed via MSLP changes, are mostly sufficient to explain the ensemble mean change of summer precipitation over most land regions in western and central Europe. The TD-pattern is characterised by a marked north-south wetting/drying gradient, with a broad zonal band with a near-neutral response. The CM-pattern on the other hand is tied to the development of high pressure with a center west of Ireland, associated with lagged warming of the North Atlantic (Haarsma et al. 2015). Underneath and to the east of this high-pressure region, extensive drying occurs, which for a broad latitude band east of Ireland accounts for almost the entire drying signal. In some regions the contributions reinforce each other while in other regions they counteract.
- Changes in the circulation-variability (CV-term) play only a marginal role in explaining the ensemble-mean precipitation signal. Possible exceptions are off the coast of France (RCM and GCM) where it may enhance the drying induced by the other components. This circulation-variability change term has a disproportionally large ensemble spread. In contrast, the uncertainty coming from changes in the mean circulation is the smallest. In the EC-Earth/RACMO ensemble studied here, the development of the high-pressure off the coast of Ireland is a much more robust feature than the change in circulation-variability.
- The RCM follows the GCM rather closely in terms of its mean precipitation response. Because the large-scale circulation changes are fairly model dependent, so will be their contribution to the precipitation signal. The methods used here may prove valuable for analysing and understanding uncertainties in coordinated regional climate-change experiments such as CORDEX or CORDEX-FPS (Giorgi et al. 2006; Coppola et al. 2018; Pichelli et al. 2021).
- If the analogue methodology is applied to monthly instead of daily data, the main separation into thermodynamic and circulation-change terms is still diagnosed correctly. Using an entirely different method based on an EOF-decomposition (used in e.g. Saffioti et al. 2017) the robustness of the results obtained with the analogues was confirmed. These alternatives based on monthly data offer the possibility to apply the analysis easily to other large climate-model ensembles.
- Large-scale circulation variability alone is not sufficient to explain the ensemble spread in precipitation trends. Although the circulation-based analogues can very well be used to explain the ensemble-mean precipitation changes in terms of its different contributions, a large fraction of the ensemble uncertainty cannot be explained. This is a simple consequence of the fact that (changes in) the natural variability of all other precipitation drivers (such as SST, soil-moisture preconditioning etc.) strongly impact the trends derived from single ensemble members.

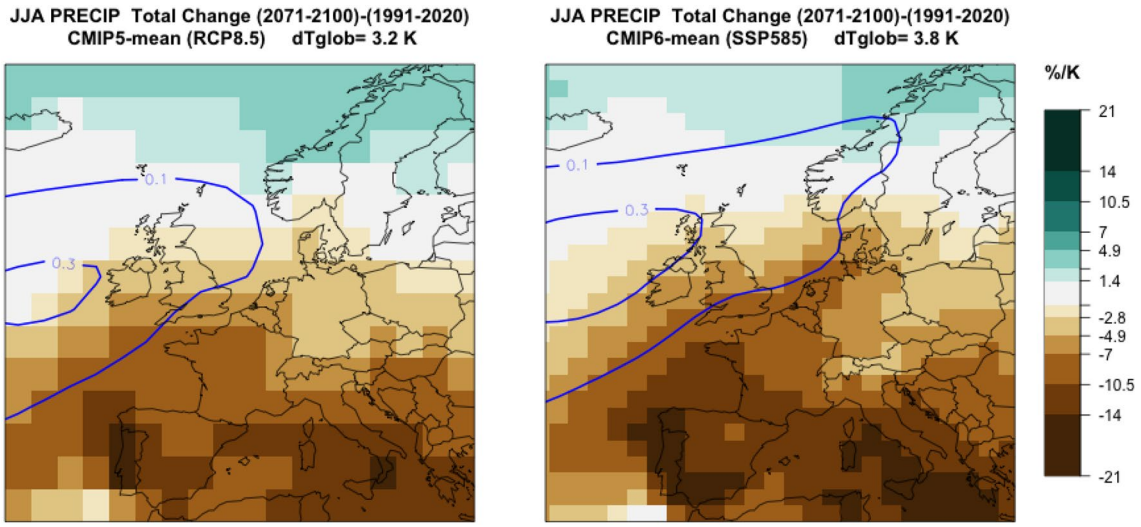


**Fig. 8** (left) Trend in CMIP5 ensemble-mean summer (JJA) precipitation and mean sea-level pressure per degree global warming. We used data from 39 CMIP5 models (Table S1). (right) Same as left panel but for the ensemble-mean of CMIP6 SSP585 (40 models, Table S2). If multiple ensemble members were available for a model, these were averaged prior to taking the multi-model mean (Data was retrieved via the KNMI Climate Explorer, climexp.knmi.nl. Access date: 2021-12-23)

We end this paper with some remarks. First, it is important to stress that in the existing literature various definitions of thermodynamic and dynamic contributions exist, which are often not exactly compatible and therefore may lead to different results. For example, our definitions differ from those used in Norris et al. (2019) and Pfahl et al. (2017). Both studies address extreme precipitation change. Norris et al. (2019) use an elegant method based on decomposing the local atmospheric moisture budget (that includes evaporation), while in Pfahl et al. (2017) a local scaling approach is used in which the thermodynamic term is defined via the change of the local saturation specific humidity and the dynamic term via changes in the local vertical velocity. In contrast to these studies on precipitation extremes, here we studied changes in the mean summer precipitation and the role of the large-scale circulation. Because of our focus on the large-scale circulation a methodology based on a local change relation seemed less appropriate. Other changes are grouped as "thermodynamic contributions", although strictly speaking "non large-scale circulation-change related contributions" would have been a more accurate description.

Secondly, realising that the circulation response may be model dependent, one can question the generality of the single-model results. As a partial answer to this question Fig. 8 (left panel) shows the future JJA precipitation and MSLP trend per degree global warming as derived from the ensemble-mean of 39 RCP8.5 CMIP5 models (Taylor et al. 2012). A similar pattern with even stronger drying trends was derived for a subset of 40 CMIP6 models and SSP585 scenario (right panel). Both patterns are remarkably similar to that of EC-Earth. Thus, even the multi-model mean fields show a clear MSLP increase west of Ireland, although due to model differences (in for example the exact location of the high) the increase is smaller than in EC-Earth. This result shows that large-scale circulation change will likely be a relevant factor and affect the future European summer precipitation climate.

Finally, the approach used in this paper connects naturally to the pseudo global warming (PGW) approach that has been used in modelling regional climate-change (Schär et al. 1996; Brogli et al. 2019a). Such approaches lead to high signal-to-noise ratios by (almost) keeping the same large-scale weather variability while including altered thermodynamics and a modified mean circulation (e.g.Pfahl et al. 2017; Lenderink et al. 2019). Using the terminology of the present study, the CV-term and the $\delta$-term (that introduces uncertainties derived from the natural variability of other drivers) are virtually absent in a PGW experiment. The present study provides a quantitative underpinning of why the signal-to-noise ratios in such PGW experiments are generally so much higher than in conventional climate-model simulations, without altering the projected total change too much.

## Appendix: Bias adjusted equations

Here we derive a set of bias-adjusted equations. Let the ensemble-mean bias of the future and present-day EPA be denoted by $\langle \varepsilon_F^e \rangle$ and $\langle \varepsilon_P^e \rangle$ respectively (similar for the type-a

and type-b analogues). By subtracting these from Eq. (3) it follows that

$$\Delta X^{fw}_{TD} = (F^a - C^e) - \left(\left\langle \varepsilon^a_F \right\rangle - \left\langle \varepsilon^e_C \right\rangle\right), \quad \text{(forward-only)} \tag{7a}$$

$$\Delta X^{bw}_{TD} = (F^e - C^a) - \underbrace{\left(\left\langle \varepsilon^e_F \right\rangle - \left\langle \varepsilon^a_C \right\rangle\right)}_{bias-adj}, \quad \text{(backward-only)} \tag{7b}$$

are "bias-adjusted" equivalents of Eq. (3). After carrying out a similar analysis that led to Eq. (4), we now obtain

$$\Delta \tilde{X}_{TD} = \Delta X_{TD} - \left(\hat{\delta}^e + \hat{\delta}^a\right)/2, \tag{8a}$$

$$\Delta \tilde{X}_{CM} = \Delta X_{CM} - \left(\hat{\delta}^b - \hat{\delta}^a\right)/2, \tag{8b}$$

$$\Delta \tilde{X}_{CV} = \Delta X_{CV} - \underbrace{\left(\hat{\delta}^e - \hat{\delta}^b\right)/2}_{bias-adj.}, \tag{8c}$$

where $\hat{\delta}^e = \langle \varepsilon^e_F \rangle - \langle \varepsilon^e_C \rangle$ and similar definitions for $\hat{\delta}^a$ and $\hat{\delta}^b$. Combining Eq. (1) and Eq. (8) gives

$$\tilde{\delta} = \left[(F - F^e) - (C - C^e)\right] + \underbrace{\hat{\delta}^e}_{bias-adj.} \tag{9}$$

Equation (9) vanishes in the ensemble mean. To solve Eqs. (8–9) we need to determine the bias of the analogues. The EPA bias is determined as the ensemble mean of Eq. (2). However, there is no direct way to determine the biases of the forward and backward analogues, because they require additional simulations. Fortunately the biases appear in the final equations only in the form of differences, so the error tends to be smaller than the bias itself. One option is therefore to ignore bias-adjustment altogether, equivalent to taking $\hat{\delta}^{e,a,b} = 0$ in Eqs. (8–9) which makes them identical to Eqs. (4–5) of the main text. In this paper we use another approach and take $\langle \varepsilon^{a,b}_{F,P} \rangle = \langle \varepsilon^e_{F,P} \rangle$ i.e., we assume that the biases of the forward and backward analogues are similar to those of the EPA. A small error is made because the circulations are not identical, but it seems more justifiable than using no bias adjustment, or applying it only to the EPA. Note that our choice implies that $\hat{\delta}^{a,b} = \hat{\delta}^e$ and therefore that, when using Eq. (8), only the TD-term in Eq. (4) is modified.

**Supplementary Information** The online version contains supplementary material available at https://doi.org/10.1007/s00382-022-06250-z.

**Acknowledgements** The authors thank the editor and two anonymous reviewers for their constructive and relevant comments on the manuscript. The authors acknowledge the HORIZON 2020 EUCP (European Climate Prediction System) project (grant agreement No. 776613, https://www.eucp-project.eu). Furthermore we acknowledge the use of the KNMI Climate Explorer (climexp.knmi.nl) for access to the CMIP5 and CMIP6 ensemble-mean fields, and the E-OBS dataset from the EU-FP6 project UERRA (http://www.uerra.eu) and the Copernicus Climate Change Service, and the data providers in the ECA&D project (https://www.ecad.eu).

**Author Contributions** The initial approach was formulated by HdV together with GL. EvM was responsible for the RCM simulations. HdV carried out the analyses and discussed results with all co-authors. The manuscript was prepared by HdV. GL, KvdW and EvM commented extensively on early drafts.

**Funding** We received funding from the HORIZON 2020 EUCP (European Climate Prediction System) project (https://www.eucp-project.eu), grant agreement No. 776613).

**Availability of data and materials** Model data is available upon reasonable request. Contact corresponding author. Gridded E-OBS data can be downloaded free of charge.

**Code availability** Code is available upon reasonable request. Contact corresponding author.

## Declarations

**Conflict of interest** Not applicable.



## References

Aalbers EE, Lenderink G, van Meijgaard E, van den Hurk BJJM (2018) Local-scale changes in mean and heavy precipitation in western Europe, climate change or internal variability? Clim Dyn 50(11):4745–4766. https://doi.org/10.1007/s00382-017-3901-9

Attema JJ, Lenderink G (2014) The influence of the North Sea on coastal precipitation in the Netherlands in the present-day and future climate. Clim Dyn 42(1–2):505–519. https://doi.org/10.1007/s00382-013-1665-4

Bladé I, Liebmann B, Fortuny D, van Oldenborgh GJ (2012) Observed and simulated impacts of the summer NAO in Europe: implications for projected drying in the Mediterranean region. Clim Dyn 39(3):709–727. https://doi.org/10.1007/s00382-011-1195-x

Brogli R, Kröner N, Sørland SL, Lüthi D, Schär C (2019a) The role of Hadley circulation and lapse-rate changes for the future European summer climate. J Clim 32(2):385–404. https://doi.org/10.1175/JCLI-D-18-0431.1

Brogli R, Sørland SL, Kröner N, Schär C (2019b) Causes of future Mediterranean precipitation decline depend on the season. Environ Res Lett. https://doi.org/10.1088/1748-9326/ab4438

Chen CT, Knutson T (2008) On the verification and comparison of extreme rainfall indices from climate models. J Clim 21(7):1605–1621. https://doi.org/10.1175/2007JCLI1494.1

Clemins PJ, Bucini G, Winter JM, Beckage B, Towler E, Betts A, Cummings R, Queiroz HC (2019) An analog approach for weather estimation using climate projections and reanalysis data. J Appl Meteorol Climatol 58(8):1763–1777. https://doi.org/10.1175/JAMC-D-18-0255.1

Coppola E, Sobolowski S, Pichelli E, Raffaele F, Ahrens B, Anders I, Ban N, Bastin S, Belda M, Belusic D, Caldas-Alvarez A, Cardoso RM, Davolio S, Dobler A, Fernandez J, Fita L, Fumiere Q, Giorgi F, Goergen K, Güttler I, Halenka T, Heinzeller D, Hodnebrog Ø, Jacob D, Kartsios S, Katragkou E, Kendon E, Khodayar S, Kunstmann H, Knist S, Lavín-Gullón A, Lind P, Lorenz T, Maraun D, Marelle L, van Meijgaard E, Milovac J, Myhre G, Panitz HJ, Piazza M, Raffa M, Raub T, Rockel B, Schär C, Sieck K, Soares PMM, Somot S, Srnec L, Stocchi P, Tölle MH, Truhetz H, Vautard R, de Vries H, Warrach-Sagi K (2018) A first-of-its-kind multi-model convection permitting ensemble for investigating convective phenomena over Europe and the Mediterranean. Clim Dyn 1:10. https://doi.org/10.1007/s00382-018-4521-8

Cornes RC, van der Schrier G, van den Besselaar EJ, Jones PD (2018) An Ensemble Version of the E-OBS Temperature and Precipitation Data Sets. J Geophys Res Atmos 123(17):9391–9409. https://doi.org/10.1029/2017JD028200

Coumou D, Di Capua G, Vavrus S, Wang L, Wang S (2018) The influence of Arctic amplification on mid-latitude summer circulation. Nat Commun. https://doi.org/10.1038/s41467-018-05256-8 (http://link.springer.com/10.1007/s40641-018-0105-2)

Deser C, Lehner F, Rodgers KB, Ault T, Delworth TL, DiNezio PN, Fiore A, Frankignoul C, Fyfe JC, Horton DE, Kay JE, Knutti R, Lovenduski NS, Marotzke J, McKinnon KA, Minobe S, Randerson J, Screen JA, Simpson IR, Ting M (2020) Insights from Earth system model initial-condition large ensembles and future prospects. Nat Clim Change 10(4):277–286. https://doi.org/10.1038/s41558-020-0731-2

Fereday D, Chadwick R, Knight J, Scaife AA (2018) Atmospheric dynamics is the largest source of uncertainty in future winter European rainfall. J Clim 31(3):963–977. https://doi.org/10.1175/JCLI-D-17-0048.1

Fowler HJ, Lenderink G, Prein AF, Westra S, Allan RP, Ban N, Barbero R, Berg P, Blenkinsop S, Do HX, Guerreiro S, Haerter JO, Kendon EJ, Lewis E, Schaer C, Sharma A, Villarini G, Wasko C, Zhang X (2021) Anthropogenic intensification of short-duration rainfall extremes. Nat Rev Earth Environ 2(2):107–122. https://doi.org/10.1038/s43017-020-00128-6

Giorgi F, Jones C, Asrar GR (2006) Addressing climate information needs at the regional level: the CORDEX framework. Bull Am Meteorol Soc 58:175–183

Haarsma RJ, Selten F, Hurk BV, Hazeleger W, Wang X (2009) Drier Mediterranean soils due to greenhouse warming bring easterly winds over summertime central Europe. Geophys Res Lett 36(4):1–7. https://doi.org/10.1029/2008GL036617

Haarsma RJ, Selten FM, Drijfhout SS (2015) Decelerating Atlantic meridional overturning circulation main cause of future west European summer atmospheric circulation changes. Environ Res Lett. https://doi.org/10.1088/1748-9326/10/9/094007

Hazeleger W, Wang X, Severijns C, Stefanescu S, Bintanja R, Sterl A, Wyser K, Semmler T, Yang S, van den Hurk BJM, van Noije T, van der Linden E, van der Wiel K (2012) EC-EARTH V2.2: description and validation of a new seamless Earth system prediction model. Clim Dyn 39:2611–2629. https://doi.org/10.1007/s00382-011-1228-5

Holton JR (1979) An introduction to dynamic meteorology, 2nd edn. Academic Press Inc, Berlin

Lehner F, Deser C, Maher N, Marotzke J, Fischer EM, Brunner L, Knutti R, Hawkins E (2020) Partitioning climate projection uncertainty with multiple large ensembles and cmip5/6. Earth Syst Dyn 11(2):491–508 https://doi.org/10.5194/esd-11-491-2020,https://esd.copernicus.org/articles/11/491/2020/

Lenderink G, Meijgaard E, Selten F (2009) Intense coastal rainfall in the Netherlands in response to high sea surface temperatures: analysis of the event of August 2006 from the perspective of a changing climate. Clim Dyn 32(1):19–33. https://doi.org/10.1007/s00382-008-0366-x

Lenderink G, Belusic D, Fowler HJ, Kjellstrom E, Lind P, van Meijgaard E, van Ulft B, de Vries H (2019) Systematic increases in the thermodynamic response of hourly precipitation extremes in an idealized warming experiment with a convection-permitting climate model. Environ Res Lett. https://doi.org/10.1088/1748-9326/ab214a

Meehl G, Stocker T, Collins W, Friedlingstein P, Gaye A, Gregory JM, Kitoh A, Knutti R, Murphy JM, Noda A, Raper S, Watterson I, Weaver A, Zhao ZC (2007) Global climate projections. In: Solomon S, Qin D, Manning M, Chen Z, Marquis M, Averyt KB, Tignor M, Miller HL (eds) Climate Change 2007: the physical science basis. Contribution of Working Group I to the Fourth Assessment Report of the Intergovernmental Panel on Climate Change. Cambridge University Press, Cambridge

Meinshausen M, Smith S, Calvin K, Daniel J, Kainuma M, Lamarque JF, Matsumoto K, Montzka S, Raper S, Riahi K, Thomson A, Velders G, van Vuuren D (2011) The RCP greenhouse gas concentrations and their extensions from 1765 to 2300. Clim Change 109:213–241. https://doi.org/10.1007/s10584-011-0156-z

Norris J, Chen G, Neelin JD (2019) Thermodynamic versus dynamic controls on extreme precipitation in a warming climate from the community earth system model large ensemble. J Clim 32(4):1025–1045. https://doi.org/10.1175/JCLI-D-18-0302.1

O'Gorman PA, Schneider T (2009) The physical basis for increases in precipitation extremes in simulations of 21st century climate change. Proc Natl Acad Sci USA 106:14773–14777. https://doi.org/10.1073/pnas.0907610106

Pfahl S, O'Gorman PA, Fischer EM (2017) Understanding the regional pattern of projected future changes in extreme precipitation. Nat Clim Change. https://doi.org/10.1038/nclimate3287

Pichelli E, Coppola E, Sobolowski S, Ban N, Giorgi F, Stocchi P, Alias A, Belušić D, Berthou S, Caillaud C, Cardoso RM, Chan S, Christensen OB, Dobler A, de Vries H, Goergen K, Kendon EJ, Keuler K, Lenderink G, Lorenz T, Mishra AN, Panitz HJ, Schär C, Soares PM, Truhetz H, Vergara-Temprado J (2021) The first multi-model ensemble of regional climate simulations at kilometer-scale resolution part 2: historical and future simulations of precipitation. Clim Dyn 56(11–12):3581–3602. https://doi.org/10.1007/s00382-021-05657-4

Polade SD, Pierce DW, Cayan DR, Gershunov A, Dettinger MD (2014) The key role of dry days in changing regional climate and precipitation regimes. Sci Rep 4:1–8. https://doi.org/10.1038/srep04364

Rowell DP, Jones RG (2006) Causes and uncertainty of future summer drying over Europe. Clim Dyn 27(2–3):281–299. https://doi.org/10.1007/s00382-006-0125-9

Saffioti C, Fischer EM, Knutti R (2017) Improved consistency of climate projections over Europe after accounting for atmospheric

circulation variability. J Clim 30(18):7271–7291. https://doi.org/10.1175/JCLI-D-16-0695.1

Schär C, Frei C, Lüthi D, Davies HC (1996) Surrogate climate-change scenarios for regional climate models. Geophys Res Lett 23(6):669–672. https://doi.org/10.1029/96GL00265

Sippel S, Meinshausen N, Merrifield A, Lehner F, Pendergrass AG, Fischer E, Knutti R (2019) Uncovering the forced climate response from a single ensemble member using statistical learning. J Clim 32(17):5677–5699. https://doi.org/10.1175/JCLI-D-18-0882.1

Taylor KE, Stouffer RJ, Meehl GA (2012) An Overview of CMIP5 and the experiment design. Bull Am Meteorol Soc 93:485–498. https://doi.org/10.1175/BAMS-D-11-00094.1

Van der Wiel K, Bintanja R (2021) Contribution of climatic changes in mean and variability to monthly temperature and precipitation extremes. Commun Earth Environ. https://doi.org/10.1038/s43247-020-00077-4

van Haren R, van Oldenborgh GJ, Lenderink G, Collins M, Hazeleger W (2012) SST and circulation trend biases cause an underestimation of European precipitation trends. Clim Dyn. https://doi.org/10.1007/s00382-012-1401-5

van Haren R, Haarsma RJ, de Vries H, van Oldenborgh GJ, Hazeleger W (2015) Resolution dependence of circulation forced future central European summer drying. Environ Res Lett 10(5):055,002, https://doi.org/10.1088/1748-9326/10/5/055002, http://stacks.iop.org/1748-9326/10/i=5/a=055002?key=crossref.25604ac229981776bde5c8bf02895525

van Meijgaard E, van Ulft L, van de Berg W, Bosveld F, van den Hurk BJM, Lenderink G, Siebesma A (2008) The KNMI regional atmospheric climate model RACMO, version 2.1. Tech. Rep. TR-302, KNMI, https://www.knmi.nl/kennis-en-datacentrum/publicatie/the-knmi-regional-atmospheric-climate-model-racmo-version-2-1. Accessed June 2021

van Meijgaard E, van Ulft LH, Lenderink G, de Roode SR, Wipfler L, Boers R, Timmermans RMA (2012) Refinement and application of a regional atmospheric model for climate scenario calculations of Western Europe. KvR 054/12, ISBN/EAN 978-90-8815-046-3, Climate changes Spatial Planning, https://library.wur.nl/WebQuery/wurpubs/fulltext/312258. Accessed June 2021

van Ulden AP, van Oldenborgh GJ (2006) Large-scale atmospheric circulation biases and changes in global climate model simulations and their importance for climate change in Central Europe. Atmos Chem Phys 6:863–881. https://doi.org/10.5194/acp-6-863-2006

...Vautard R, Kadygrov N, Iles C, Boberg F, Buonomo E, Bülow K, Coppola E, Corre L, Meijgaard E, Nogherotto R, Sandstad M, Schwingshackl C, Somot S, Aalbers E, Christensen OB, Ciarlo JM, Demory M, Giorgi F, Jacob D, Jones RG, Keuler K, Kjellström E, Lenderink G, Levavasseur G, Nikulin G, Sillmann J, Solidoro C, Sørland SL, Steger C, Teichmann C, Saqi K, Wulfmeyer V (2021) Evaluation of the Large EURO?CORDEX Regional Climate Model Ensemble. J Geophys Res Atmos 126(17):1–28. https://doi.org/10.1029/2019jd032344

Wood RR, Lehner F, Pendergrass AG, Schlunegger S (2021) Changes in precipitation variability across time scales in multiple global climate model large ensembles. Environ Res Lett. https://doi.org/10.1088/1748-9326/ac10dd

Yiou P (2014) AnaWEGE: A weather generator based on analogues of atmospheric circulation. Geosci Model Dev 7(2):531–543. https://doi.org/10.5194/gmd-7-531-2014